



# LUND UNIVERSITY

## Analysis and estimation of MIMO-SAR for multi-antenna mobile handsets

Li, Hui; Tsiaras, Apostolos; Lau, Buon Kiong

*Published in:*  
IEEE Transactions on Antennas and Propagation

*DOI:*  
[10.1109/TAP.2016.2647708](https://doi.org/10.1109/TAP.2016.2647708)

2017

*Document Version:*  
Peer reviewed version (aka post-print)

[Link to publication](#)

*Citation for published version (APA):*  
Li, H., Tsiaras, A., & Lau, B. K. (2017). Analysis and estimation of MIMO-SAR for multi-antenna mobile handsets. *IEEE Transactions on Antennas and Propagation*, 1522 - 1527.  
<https://doi.org/10.1109/TAP.2016.2647708>

*Total number of authors:*  
3

### General rights

Unless other specific re-use rights are stated the following general rights apply:  
Copyright and moral rights for the publications made accessible in the public portal are retained by the authors and/or other copyright owners and it is a condition of accessing publications that users recognise and abide by the legal requirements associated with these rights.

- Users may download and print one copy of any publication from the public portal for the purpose of private study or research.
- You may not further distribute the material or use it for any profit-making activity or commercial gain
- You may freely distribute the URL identifying the publication in the public portal

Read more about Creative commons licenses: <https://creativecommons.org/licenses/>

### Take down policy

If you believe that this document breaches copyright please contact us providing details, and we will remove access to the work immediately and investigate your claim.

LUND UNIVERSITY

PO Box 117  
221 00 Lund  
+46 46-222 00 00

# Analysis and Estimation of MIMO-SAR for Multi-antenna Mobile Handsets

Hui Li, Apostolos Tsiaras and Buon Kiong Lau

**Abstract**—Measuring MIMO-SAR is an important part of mobile handset evaluation, following the introduction of uplink MIMO transmission schemes in LTE-Advanced. However, the measurement of MIMO-SAR is complex and time-consuming. In this paper, 6 unique dual-antenna mobile handsets, including both typical and novel designs, are analyzed to determine the dependence of MIMO-SAR on antenna configuration and correlation. It is found that, for certain antenna configurations, the location of the maximum MIMO-SAR and the corresponding relative phase between the ports can be predicted. This can be applied to drastically reduce measurement time. In addition, dual-antennas with low envelope correlation coefficients in the radiation patterns also offer near-orthogonal electric near-fields. This leads to smaller MIMO-SAR than stand-alone SAR (S-SAR) over all relative phases, making MIMO-SAR measurement unnecessary. The results also provide guidelines for designing multi-antenna handsets with low SARs. For verification, the S-SAR and MIMO-SAR at relative phase of 0° were measured for several prototypes. The measured SAR distributions showed good agreement with the simulated ones.

**Index Terms**—Mobile antenna; multiple-input multiple-output (MIMO); multi-antennas; specific absorption rate (SAR).

## I. INTRODUCTION

MULTI-ANTENNA mobile prototypes have become a norm in wireless communications due to mandatory downlink MIMO capability in Long Term Evolution (LTE) systems. In addition, the newly deployed LTE-Advanced systems also include uplink MIMO transmissions, which require multiple antennas to be simultaneously excited. This means that the multi-antenna mobile prototypes must comply with international standards for limiting human exposure to radio-frequency (RF) fields. RF exposure is specified by Specific Absorption Rate (SAR), which is defined for a given point in space by [1]–[3]

$$\text{SAR} = \frac{\sigma}{\rho} |\mathbf{E}|^2, \quad (1)$$

where  $\sigma$  and  $\rho$  denote the electric conductivity and density of the tissue, respectively.  $\mathbf{E}$  is the total electric field (E-field) at that point in the tissue. For single-antenna or multi-antennas in selection diversity scheme,  $\mathbf{E}$  is simply the E-field from the excited antenna. In contrast, for multi-antenna schemes in

general (e.g., maximum ratio combining and spatial multiplexing), more than one antenna is excited. Hence,  $\mathbf{E}$  is the vector summation of the individual E-fields from the multi-antennas. Thus, the amplitudes and phases of the complex-valued E-fields depend on the MIMO precoding used. For clarity, SAR in the case of multi-antenna excitation is also named MIMO-SAR. It has been shown in [4] that the maximum MIMO-SAR changes substantially (over 50%) over different relative signal phases in the head phantom case. However, exhaustive measurement of MIMO-SAR is time-consuming and impractical. Even if there are only two antennas and the transmit power of the two antennas is set to maximum, the relative phase needs to be varied from 0° to 360°.

Several recent studies focused on evaluating and estimating SAR for multi-antennas [5]–[11]. In [5], Wang et al. provided a tighter upper bound of MIMO-SAR than one based only on electric field magnitudes, improving SAR estimation accuracy. Similarly, [6] presented three alternative schemes for combining fields from multi-antenna elements to estimate exposure levels. In [7], it was found that the relative phase difference that gives the maximum SAR only changes by a few degrees over different measurement planes, which will not change the position of the maximum local SAR. Thus, in the area scan, only the measurement plane near the inner surface of the phantom is needed. In addition, methods of determining MIMO-SAR in measurement using vector E-field probes and scalar E-field probes were proposed in [8] and [9], respectively. Moreover, studies were also carried out from the antenna perspective. The influence of the ground plane on the SAR for several dual-antenna mobile prototypes was evaluated in [10], mainly for the stand-alone SAR (S-SAR). Average MIMO-SAR (over all relative phases) was studied for 5 dual-antenna prototypes in [11], focusing on the impact of antenna type on SAR.

This paper analyzes the influence of antenna configuration and correlation on MIMO-SAR distribution for 6 dual-antenna prototypes, with the aims to reduce measurement time and to provide guidelines for low-SAR multi-antenna designs.

## II. ANTENNA CONFIGURATIONS AND SYSTEM SETUP

Figure 1 shows the 6 dual-antenna mobile prototypes used in this study. They include both conventional and novel designs. The dual antenna elements on each prototype are mounted on a 130 mm × 65 mm chassis. The small red arrows in Fig. 1 indicate the location of the antenna ports. Lumped ports were used in the simulation. All the antennas are multi-band (i.e., dual- or triple-band). At the higher band(s), due to the electrical distance between the antenna elements being larger, the interaction between antennas is weaker and MIMO-SAR is expected to be less severe. Thus, we focus on the SAR behavior at the lowest band, with the center frequency of 0.859 GHz. As indicated in Table I, the 6 prototypes were designed to provide antennas of different types, positions, and envelope correlation coefficients (ECCs) on a flat phantom (to be described later):

- Prototypes A and B are of different antenna types, with antennas symmetrically located at two shorter edges of the

Manuscript received May 31, 2016. This work was This research is funded by: (1) National natural science foundation of China (no. 61601079); (2) the Fundamental Research Funds for the Central Universities (no. DUT15RC(3)063); (3) the Swedish Research Council under grant no. 2010-468.

H. Li is with School of Information and Communication Engineering, Dalian University of Technology, Dalian, 116024, China. E-mail: [hui.li@dlut.edu.cn](mailto:hui.li@dlut.edu.cn);

A. Tsiaras is with nok9 AB, Malmo, S-211 28, Sweden. E-mail: [at@nok9.com](mailto:at@nok9.com);

B. K. Lau is with the Department of Electrical and Information Technology, Lund University, SE-221 00 Lund, Sweden. E-mail: [bkl@eit.lth.se](mailto:bkl@eit.lth.se).

chassis.

- Prototypes B and C utilize the same antennas, but with the dual-antennas located on either the same edge or different edges of the chassis. The purpose is to study the influence of the antenna arrangement.

- Prototype D uses two different antennas in one setup, with the antenna locations being the same as Prototypes A and B. Hence, the influence of the asymmetry in the antenna type can be investigated.

- Prototypes E and F are novel antenna designs that provide low ECCs, which are different from more conventional Prototypes A to D that have relatively high ECCs. The influence of ECC on SAR can be studied by comparing the two groups of prototypes.

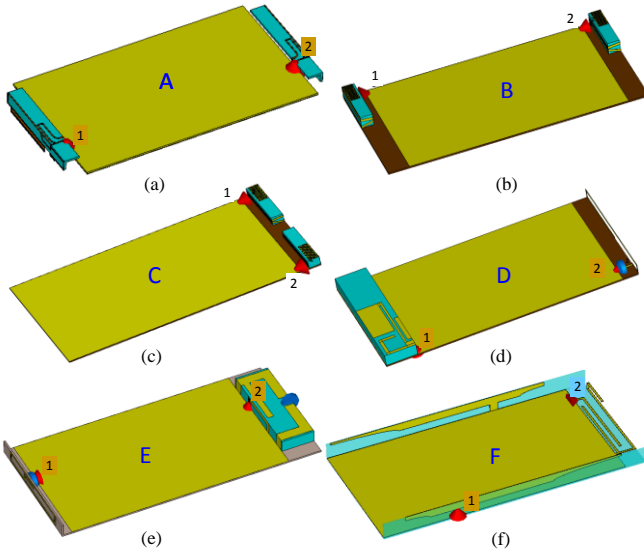


Fig. 1. Dual-antenna prototypes (A-F) with different antenna configurations.

TABLE I  
SUMMARY OF ANTENNA SETUPS

Prototype	Antenna type	Position on chassis	ECC
A	Identical inverted-F antennas (IFAs) [12]	Two shorter edges	0.41
B	Identical capacitively-fed monopoles [12]	Two shorter edges	0.47
C	Identical capacitively fed monopoles [12]	Same shorter edge	0.43
D	Monopole + planar IFA (PIFA)	Two shorter edges	0.55
E	Monopole + loop [13]	Two shorter edges	0.001
F	Monopole + T-strip [14]	One shorter edge + two longer edges	0.025

Flat phantom (i.e., body-worn scenario) is chosen in this study for two reasons. Firstly, multi-antenna excitation is used to provide high data rates, which are not needed to support a voice call (talk mode). Secondly, the effect of antennas on SAR performance can be more easily isolated in the flat phantom case due to its simple geometry. The antennas are placed 3 mm above the phantom, as presented in the inset of Fig. 3(a), representing the case where the mobile prototype is very close

to the body. Since the antennas will be detuned differently in the proximity of the body, accepted power of 24 dBm (0.25 W), which excludes the mismatch and mutual coupling factors, is used in the simulation for fair comparison.

### III. SIMULATION AND ANALYSIS

To reduce MIMO-SAR measurement time and providing guidelines for low-SAR multi-antennas design, analysis using full-wave simulations were performed on the 6 prototypes in Fig. 1 in the time-domain solver in CST Microwave Studio. The S-SAR was simulated when one port was excited with the accepted power of 24 dBm (0.25W), and the other was loaded with 50 ohms. The MIMO-SAR was evaluated when the two ports were excited simultaneously with an accepted power of 21 dBm (0.125W) at each port. The phase shift between the ports was varied from  $0^\circ$  to  $360^\circ$ . The MIMO case corresponds to the signal from a single transmitter being split into two phase-shifted components for the two antennas. Both (peak) S-SAR and MIMO-SAR results were then extracted and analyzed over 1 g tissue. The MIMO SAR for all prototypes was first normalized to the worst S-SAR (2.75 W/kg in Prototype E) and the results are presented in Fig. 2. It is observed that the co-located setup (Prototype C) gives the highest MIMO-SAR values of all prototypes, despite Prototype B having the same antenna elements and similar ECCs (0.47 vs 0.43). A closer examination revealed that the maximum S-SAR is also higher in Prototype C than B. The reason for the higher S-SAR is that the close antenna spacing in Prototype C provides each antenna with a higher total electric field (and S-SAR) in the tissue due to the significant induced field from the nearby coupled antenna. In the case of MIMO-SAR, the relatively high ECC and close antenna spacing facilitate effective constructive interference at the relative phase of  $180^\circ$ , resulting in the highest MIMO-SAR. In addition, it can be seen the variation of MIMO-SAR with respect to phase shift is significantly higher in Prototype C than in any other prototype (irrespective of antenna types and ECC). This phenomenon highlights the problem of co-located antennas being more susceptible to constructive and destructive interferences in the nearfield.

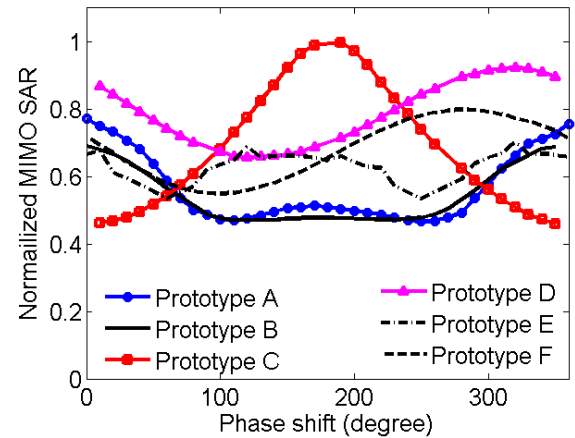


Fig. 2. Normalized MIMO-SAR vs relative phase for Prototypes A-F.

Considering that antennas of different types were employed in the prototypes, to highlight the influence of antenna

configuration and ECC, the MIMO-SAR result for each prototype was normalized to its individual maximum S-SAR value.

#### A. Dependence of SAR on Antenna Configurations

The normalized MIMO-SAR for Prototypes A-D is shown in Fig. 3, with the absolute values of the peak S-SAR for each antenna noted in the legend. From Fig. 3(a) and 3(b), it is observed that the maximum MIMO-SAR values are obtained at the relative phase of  $0^\circ$  for identical antennas located on the two shorter edges of the chassis, which is a typical setup for MIMO antennas.

To illustrate the phenomenon, the electric near fields of the antennas were simulated. Figure 4 gives the two-dimensional cut of the E-field along the length of Prototype A, with one port excited at a time. It can be seen that the E-fields are strong at the two edges of the chassis and present similar field distributions regardless of the excited antenna. This is because when electric antennas (e.g., monopoles, IFAs, PIFAs) are placed at a shorter edge of the chassis, the entire chassis becomes the main radiator [15]. The in-phase E-fields around both ports in Fig. 4 also illustrate the constructive summation of MIMO-SAR at  $0^\circ$  in Fig. 3(a) and 3(b).

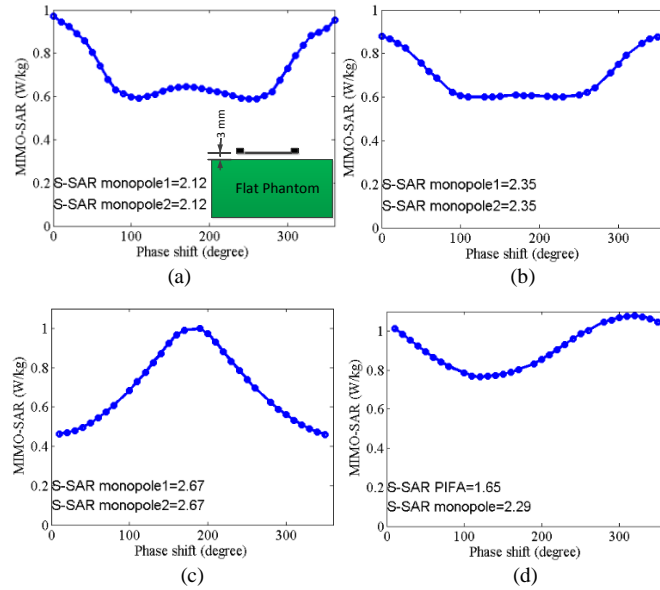


Fig. 3. Individually normalized MIMO-SAR vs relative phase and absolute S-SAR for Prototype A-D, illustrated in subplots (a)-(d), respectively.

The maximum SAR of Prototype A locates near the shorter edges of the chassis (see the SAR distributions in Table II). Prototype B and in general identical electric antennas placed in mirror symmetry along the chassis length offer similar field distributions and MIMO-SAR trends. This has been verified by antennas of various types in the simulation. The maximum MIMO-SAR for Prototype D occurs slightly away from  $0^\circ$  relative phase, since the antennas are not identical. The excitation of the chassis by both electric antennas in Prototype A to D also leads to relatively higher ECC, as shown in Table I.

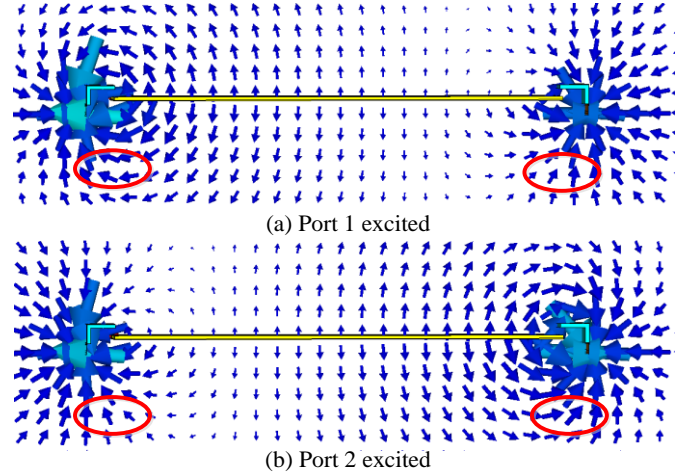


Fig. 4. E-fields along the length of the chassis for Prototype A.

For antennas placed on the same edge of the chassis, as for Prototype C, the MIMO-SAR result shows a different trend (see Fig. 3(c)). The E-field cut along the width of the chassis (at the antenna location) is provided in Fig. 5. As the antennas are in proximity of each other, a capacitance effect is formed when voltage (excitation) is applied to one antenna, with the other antenna loaded with 50 ohms. The field distribution around the gap is similar to that of a capacitor formed by parallel plates. The fields are out of phase when different antennas are excited. Thus, the maximum MIMO-SAR will be achieved at a relative phase of  $180^\circ$ , as verified by Fig. 3(c). The maximum MIMO-SAR was found to be slightly higher than the S-SAR. Reducing the distance between the antennas will lead to an even higher MIMO-SAR. However, the relative phase that gives the maximum SAR remained unchanged with the smaller antenna spacing.

From the above analysis, it can be concluded that the relative phase for maximum MIMO-SAR can be predicted for different symmetric antenna configurations. Thus, for symmetric configurations, it is possible to save MIMO-SAR measurement time by using a-priori knowledge to avoid measuring over different relative phases.

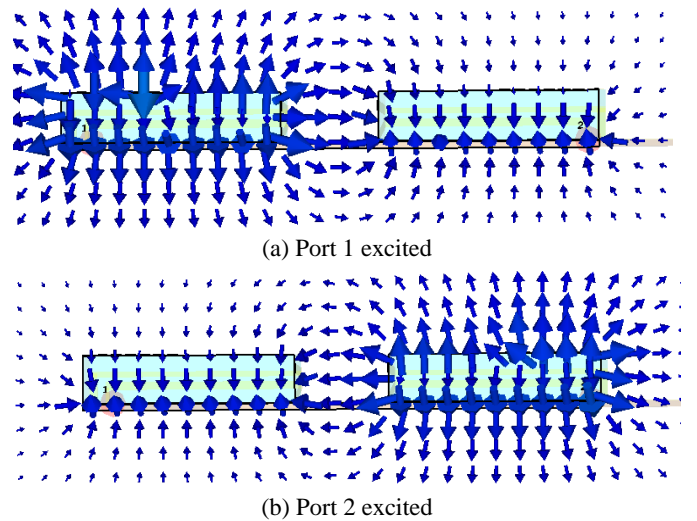


Fig. 5. E-fields along the width of the chassis for Prototype C



In practice, many factors, such as components on the chassis and power handling, can cause the antenna setup to deviate from being symmetric. To study the influence of asymmetrical chassis, a speaker and a battery (modeled by full-metal structures) were added to the chassis, as shown in Fig. 6. Furthermore, the structures were intentionally placed very close (3 mm) to the antennas. It was found that the symmetrical SAR distribution *vs* relative phase is almost unchanged. Thus, the effect of those disturbances on the chassis is limited.

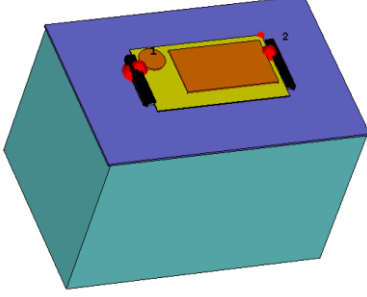


Fig. 6. Configuration of Prototypes A with speaker and battery

Different power handling was also investigated for Prototype A. Rather than dividing the power equally, the power fed into port 1 was set to be half of the power fed into port 2, with the total accepted power kept the same. The absolute MIMO-SAR values with different relative phases are presented in Fig. 7. It can be seen that the curve is not as symmetrical as before. However, the maximum MIMO-SAR is still obtained at a relative phase of  $0^\circ$ . This indicates that moderate power imbalance may only have limited impact on the relative phase for maximum MIMO-SAR.

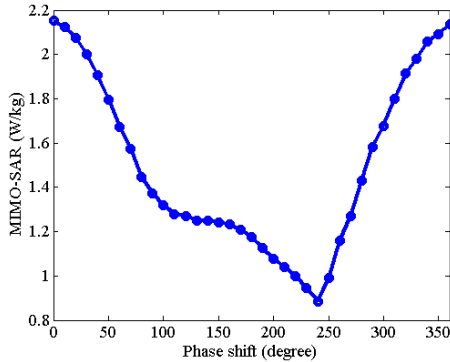


Fig. 7. Absolute MIMO-SAR values *vs* relative phase for Prototype A with power distribution of 1:2 over the ports.

#### B. Dependence of SAR on ECC

Due to shared chassis excitation by both antenna elements, the ECCs for Prototypes A to D are above 0.4 (see Table I), regardless of the antenna types and positions. To reduce the ECC, different strategies were proposed: 1) Prototype E employs a capacitively fed loop at one shorter edge to form a magnetic antenna that has orthogonal pattern to the monopole antenna [13]; 2) Prototype F uses a T-strip antenna to excite the transversal dipole mode along the chassis width, which is not correlated to the longitude dipole mode excited by the monopole [14]. The ECCs for both prototypes are below 0.03 at

the center frequency.

Similar as Prototypes A to D, the normalized MIMO-SAR for Prototypes E and F are shown in Fig. 8. The normalized MIMO-SAR in Fig. 8(a) shows that its maximum SAR value is only 70% of the maximum S-SAR, owing to the fully de-correlated radiation patterns. The E-field of the loop antenna in Prototype E is presented in Fig. 9, which is pointing into the paper. The field distribution of the monopole is not shown as it is similar to Fig. 4(b), i.e., the field vector is along the paper plane. Thus, the E-field vectors of the two antennas are always perpendicular to each other regardless of their relative phase, and hence the total field is far smaller than the summation of their field magnitudes. Similarly, the low ECC for Prototype F is reflected in the orthogonal E-field distributions of the two antennas, resulting in MIMO-SAR to be smaller than S-SAR. Hence, designing MIMO antennas with low correlation not only provides better system performance (e.g. capacity), but it can also provide lower MIMO-SAR values. Moreover, since S-SAR is found to be always higher than MIMO-SAR, only S-SAR needs to be measured for SAR evaluation.

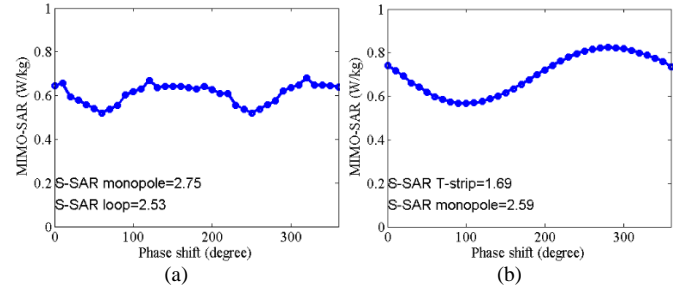


Fig. 8. Normalized MIMO-SAR *vs* relative phase and absolute S-SAR for Prototypes E and F, illustrated in subplots (a) and (b), respectively.

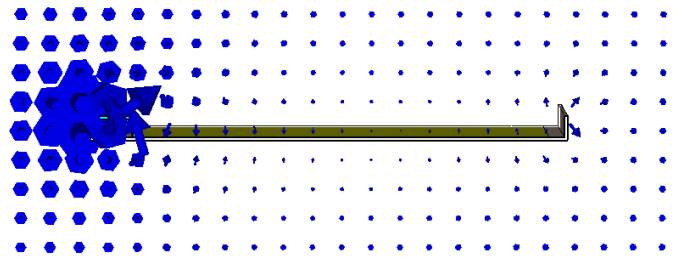


Fig. 9. E-field along the length of the chassis for the loop antenna in Prototype E.

#### IV. PROTOTYPES AND EXPERIMENTS

The antenna prototypes in the simulations were fabricated to verify the SAR distributions. The measurement setup of the flat phantom is presented in Fig. 10. A signal is first generated and amplified, and then transmitted through a directional coupler. To ensure that the accepted power by the antenna is kept at 0.25W, a power monitor is used at P3. For the S-SAR measurement, the signal from P2 is directly connected to one port of the antenna, with the other port loaded with 50 ohms. For MIMO-SAR measurements, a splitter is used to transmit equal power to the two ports through cables of the same length, representing the case of  $0^\circ$  relative phase.

The simulated and measured results of SAR distribution are shown in Tables II and III, with Prototypes A and F as representative cases. In general, the measurement results agree well with the simulated ones. For Prototype A, the measured maximum S-SAR and MIMO-SAR ( $0^\circ$  relative phase) are 1.96 W/kg and 1.68 W/kg, respectively, which are lower than the simulated values shown in Fig. 2 (a). The difference between SAR distributions could be due to the probe not being exactly positioned in the plane with the maximum SAR values. Other factors, such as tolerance of tissue-simulating liquid properties, prototype fabrication and cable effects, could also contribute to the discrepancy. It is observed that simulated and measured MIMO-SAR have larger discrepancies than the S-SAR counterpart. This is partly attributed to the  $0^\circ$  phase difference not being easy to obtain in the measurement. A more sophisticated way to obtain an accurate relative phase is provided in [16]. In addition, a slight asymmetry in the measured SAR distribution is observed for Prototype A (see Table II). However, it was shown in Section III-A that some asymmetries in the antenna setup (that can lead to the asymmetric SAR distribution) have limited impact on maximum MIMO-SAR being obtained at  $0^\circ$  relative phase for symmetrically placed electric antennas on the chassis.

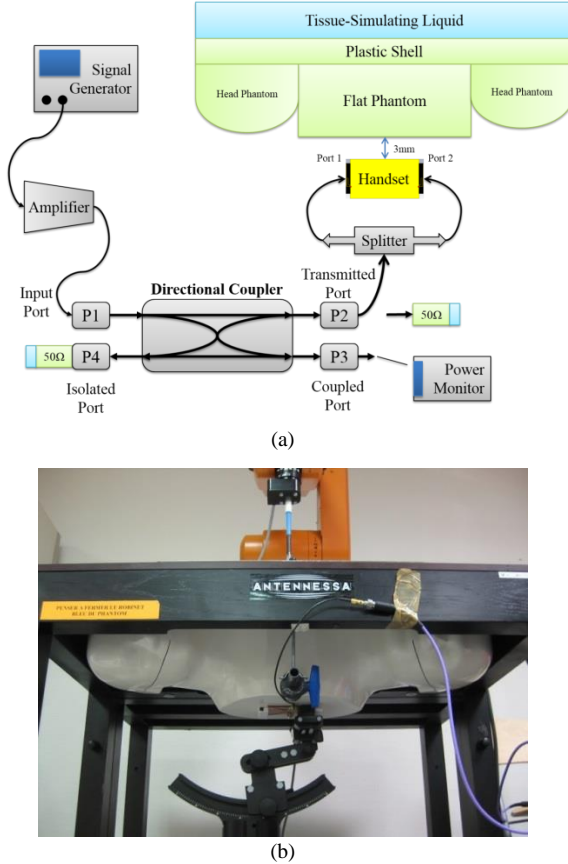


Fig. 10. (a) Block diagram and (b) photo of SAR measurement setup.

The measured MIMO-SAR ( $0^\circ$  relative phase) for Prototype F is 2.03 W/kg, which is slightly higher than the simulated value. This is because in the simulation, the accepted power could be perfectly controlled to exclude impedance matching

and mutual coupling effects. However, in the measurement, the input power was estimated from the measured impedance matching, coupling and the required accepted power, which introduced some errors. Therefore, some discrepancies can be expected between the actual accepted power by each antenna and the targeted power. Moreover, the fabricated prototypes are not exactly the same as those simulated due to tolerances in fabrication, material properties as well as cable effects, as illustrated in [12] and [14] for Prototypes A and F, respectively. All of these factors can contribute to either larger or smaller measured peak SAR relative to the simulated value.

TABLE II  
SIMULATED AND MEASURED SAR DISTRIBUTIONS FOR PROTOTYPE A

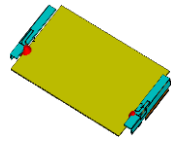
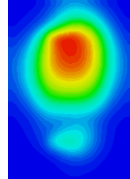
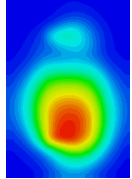
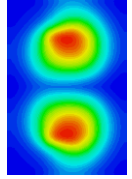
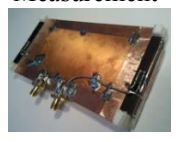
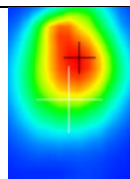
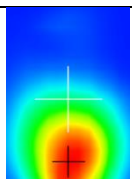
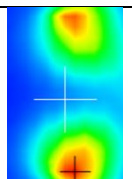

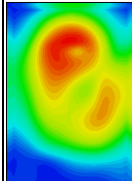
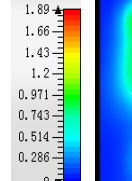
Prototype A	S-SAR		MIMO-SAR
	Port 1	Port 2	$\Delta\phi=0^\circ$
Simulation 			
Maximum SAR(W/kg)	2.12	2.12	2.01
Measurement 			
Maximum SAR(W/kg)	1.89	1.96	1.75

TABLE III  
SIMULATED AND MEASURED SAR DISTRIBUTIONS FOR PROTOTYPE F

Prototype F	MIMO-SAR ( $\Delta\phi=0^\circ$ )	
	Simulation	Measurement
		
Maximum SAR(W/kg)	1.89	2.03

## V. CONCLUSION

The MIMO-SAR performances of 6 different dual-antenna prototypes were analyzed for a body-worn scenario. Antenna configurations and correlation were the key parameters of this study. Several conclusions can be drawn from the results:

- Antennas co-located on the same chassis edge give higher SAR values than non-located ones, for both S-SAR and MIMO-SAR. The variation of MIMO-SAR over different relative phase for co-located set-ups is larger due to stronger constructive and destructive effects.
- As long as the antenna belongs to electric antennas (most of the antennas used in mobile phones are electric antennas, such as PIFA, dipole and monopole), and they

are symmetrically placed on the chassis, maximum MIMO-SAR is achieved at  $0^\circ$  relative phase for identical antennas positioned on the two shorter edges of the chassis, whereas it is obtained at  $180^\circ$  relative phase for those collocated on the same edge of the chassis.

- For symmetric antenna configurations where the dual-antennas are either placed on the two shorter edges of the chassis or collocated at one shorter edge, the measurement of maximum MIMO-SAR is only needed near a shorter edge of the chassis for a certain phase shift that can be predicted a-priori.
- Dual-antennas with low correlation give lower MIMO-SAR than S-SAR, implying that only S-SAR needs to be measured for these dual-antenna prototypes. This applies to both beamforming and spatial multiplexing scenarios.

These findings can be applied to simplify the MIMO-SAR measurement and to design antennas that can offer lower MIMO-SAR.

## REFERENCES

- [1] IEC/TR 62630, "Guidance for Evaluating Exposure from Multiple Electromagnetic Sources", Ed. 1.0, 2010.
- [2] IEC 62209-2, "Human exposure to radio frequency fields from hand-held and body-mounted wireless communication devices: Human models, instrumentation, and procedures Part 2: Procedure to determine the specific absorption rate (SAR) for wireless communication devices used in close proximity to the human body (frequency range of 30 MHz to 6 GHz)", Ed. 1.0, 2010.
- [3] IEEE 1528, "IEEE Recommended Practice for Determining the Peak Spatial-Average Specific Absorption Rate (SAR) in the Human Head from Wireless Communications Devices: Measurement Techniques", Ed. 2013.
- [4] K.-C. Chim, K. C. L. Chan, and R. D. Murch, "Investigating The Impact of Smart Antennas on SAR", *IEEE Trans. Antennas Propag.*, vol. 52, no. 5, 1370-1374, May 2004.
- [5] M. S. Wang, L. Lin, J. Chen, D. Jackson, W. Kainz, Y. H. Qi, and P. Jarmuszewski, "Evaluation and optimization of the Specific Absorption Rate for multiantenna systems," *IEEE Trans. Electromagn. Compat.*, vol. 53, pp. 628-637, Aug. 2011.
- [6] N. Perentos, S. Iskra, A. Faraone, R. J. McKenzie, G. Bit-Babik, and V. Anderson, "Exposure compliance methodologies for Multiple Input Multiple Output (MIMO) enabled networks and terminals," *IEEE Trans. Antennas Propag.*, vol. 60, pp. 644-653, Feb. 2012.
- [7] D. T. Le and V. H. Chu, "Analyses on the maximum local specific absorption rate of multiple antenna devices in different measurement planes," in *Proc. IEEE Conf. Advanced Technol. Commun. (ATC'2015)*, Ho Chi Minh, Vietnam, Oct. 14-16, 2015, pp. 496-500.
- [8] D. T. Le, L. Hamada, S. Watanabe, and T. Onishi, "An Estimation Method for Vector Probes Used in Determination SAR of Multiple-Antenna Transmission Systems" in *Proc. Int. Symp. On Electromagnetic Compatibility (EMC14)*, Tokyo, Japan, May. 2014
- [9] D. T. Le, L. Hamada, S. Watanabe, and T. Onishi, "Measurement Procedure to Determine SAR of Multiple Antenna Transmitters Using Scalar Electric Field Probes", in *Proc. of the IEEE Conf. Advanced Technol. Commun. (ATC'2014)*, Hanoi, Vietnam, Oct., 2014.
- [10] K. Zhao, S. Zhang, Z. Ying, T. Bolin, and S. He, "SAR study of different MIMO antenna designs for LTE application in smart mobile prototypes," *IEEE Trans. Antennas Propag.*, vol. 61, pp. 3270-3279, Jun. 2013.
- [11] H. Li, A. Tsiraras, B. Derat, and B. K. Lau, "Analysis of SAR on flat phantom for different multi-antenna mobile terminals," in *Proc. 8<sup>th</sup> Europ. Conf. Antennas Propag. (EuCAP'2014)*, The Hague, The Netherlands, Apr. 6-10, 2014, pp. 1989-1993.
- [12] I. Vasilev, V. Plicanic, and B. K. Lau, "Impact of antenna design on MIMO performance for compact terminals with adaptive impedance matching" *IEEE Trans. Antennas Propag.*, vol. 64, no. 4, pp. 1454-1465, Apr. 2016.
- [13] H. Li, B. K. Lau, Z. Ying and S. He, "Decoupling of multiple antennas in terminals with chassis excitation using polarization diversity, angle diversity and current control," *IEEE Trans. Antennas Propag.*, vol. 60, no. 12, pp. 490-502, Dec. 2012.
- [14] Z. Miers, H. Li, and B. K. Lau, "Design of bandwidth enhanced and multiband MIMO antennas using characteristic modes," *IEEE Antennas Wireless Propag. Lett.*, vol. 12, pp. 1696-1699, 2013.
- [15] H. Li, Y. Tan, B. K. Lau, Z. Ying and S. He, "Characteristic mode based tradeoff analysis of antenna- chassis interactions for multiple antenna terminals," *IEEE Trans. Antennas Propag.*, vol. 60, pp. 490-502, Feb. 2012.
- [16] D. T. Le, L. Hamada, S. Watanabe, and T. Onishi, "A Method in Determination of the Specific Absorption Rate of Multi-Antenna Devices" in *Proc. IEEE Int. Symp. Antennas Propag.(APS 2014)*, Memphis, US, Jul., 2014